O-doped zig-zag molecular ribbons

Andrey Berezin, Nicolas Biot, Tommaso Battisti, and Davide
Bonifazi*

[*] Dr A. Berezin, N. Biot, T. Battisti, Prof. Dr D. Bonifazi
   School of Chemistry, Cardiff University, Main Building, Park
   Place, Cardiff CF10 3AT, United Kingdom; E-mail:
   bonifazid@cardiff.ac.uk

Supporting information for this article is available on the WWW
under http://www.angewandte.org or from the author.
Crystallographic data (excluding structure factors) for the
structures reported in this paper have been deposited at the
Cambridge Crystallographic Data Centre as supplementary
publication for compounds **6** (1824268), **1** (1824269), **11** (1824270)
and **5** (1828142).

Abstract: The synthesis of the first zig-zag O-doped molecular rhombic ribbon has been achieved. This includes oxidative C-C and C-O bond formations that allowed the stepwise elongation and planarization of a oxa-congener of 2,7-periacenoacene. X-ray diffraction analysis corroborated the flat structure and the zig-zag topology of the O-doped edges. Photophysical and electrochemical investigations showed that the extension of the PXX into the molecular ribbon induces a noticeable shrinking of the molecular band gap devised by a rising of the HOMO energy level, a desirable property for *p*-type organic semiconductors.

Figure to the table of content.

2
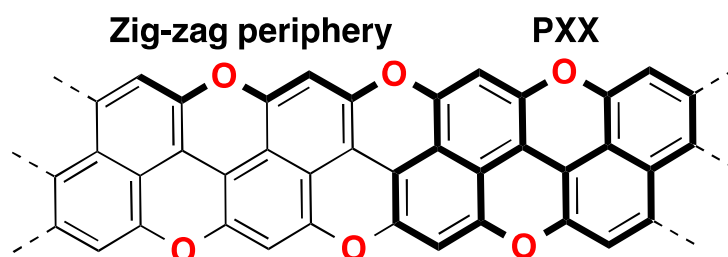
Inspired by the silicon-based technologies, the doping route is recently affirming as an effective strategy to prepare organic semiconductors with tailored optoelectronic properties.[1] The controlled replacement of carbon atoms with isostructural heteroatoms[2] gives access to congeners of size-defined molecular graphenes.[3] In particular, the isolation of extended polycyclic aromatic hydrocarbons (PAHs) featuring zig-zag edges[4] such as *m*,*n*-perifusenes (Fig. 1, *m* and *n* designates the number of fused rings)[5] is challenging owing to their susceptibility toward O_2.[6] Consequently, the preparation of archetypal zig-zag full-carbon scaffolds has been restricted so far to individual molecules under UHV conditions.**[7]** *m*,*n*-Periacenes are rectangular graphene-like nanoflakes exhibiting orthogonal zig-zag and armchair edges and derive from the fusion of a m number of [*n*]acenes[6a, 8] at their peri-position. On the other hand, *m*,*n*-periacenoacenes are rhombic nanographenes with a 60° angle featuring two zig-zag peripheries (Fig. 1). Among those, extended *m*,*n*-periacenoacenes are certainly the rarest examples.

peri*-condensed benzenoids (perifusenes)
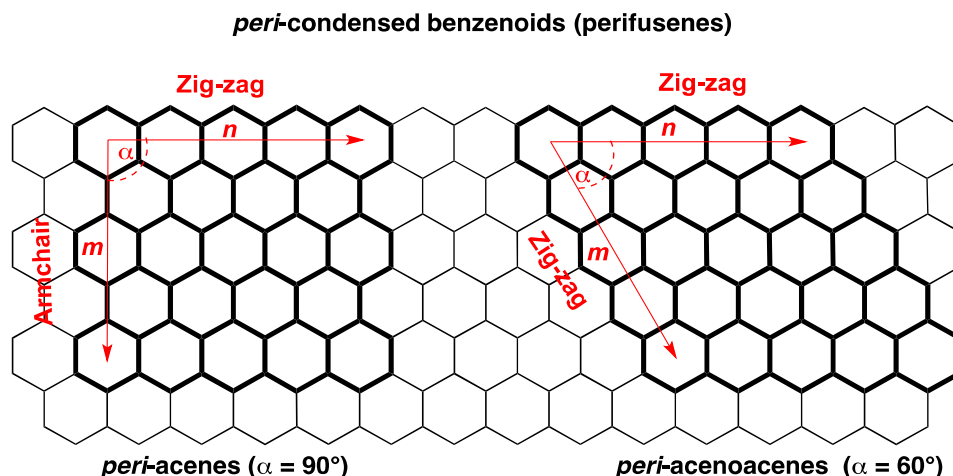
Fig. 1. Peri-acenes and peri-acenoacenes nanographenes: armchair/zig-zag (left) and zig-zag/zig-zag (right) topologies.

The substitution of the carbon edges with heteroatoms[9] has provided a viable approach to prepare stable extended PAHs featuring zig-zag peripheries, and noticeable examples included O-,[10] N-,[11] OBO-,[12] NBN-[13] and BNB-doped[14] structures. Amongst those, Pummerer's *peri*-xanthenoxanthene (PXX),[15] the O-doped

congener of anthanthrene, is certainly one of the oldest examples. The replacement of the C11 and C12 carbon atoms with oxygen atoms provides chemically stable derivatives,[10a, 10b, 16] which can be used as *p*-type semiconductors.[17] Building on this structural motif, one can conjecture that this approach could lead to PAHs featuring extended zig-zag peripheries. Indulging this line of thought, herein we put forward the first synthesis of a O-doped congener of 2,7-periacenoacene, in which six carbon atoms at the zig-zag edges have been replaced by oxygen atoms.
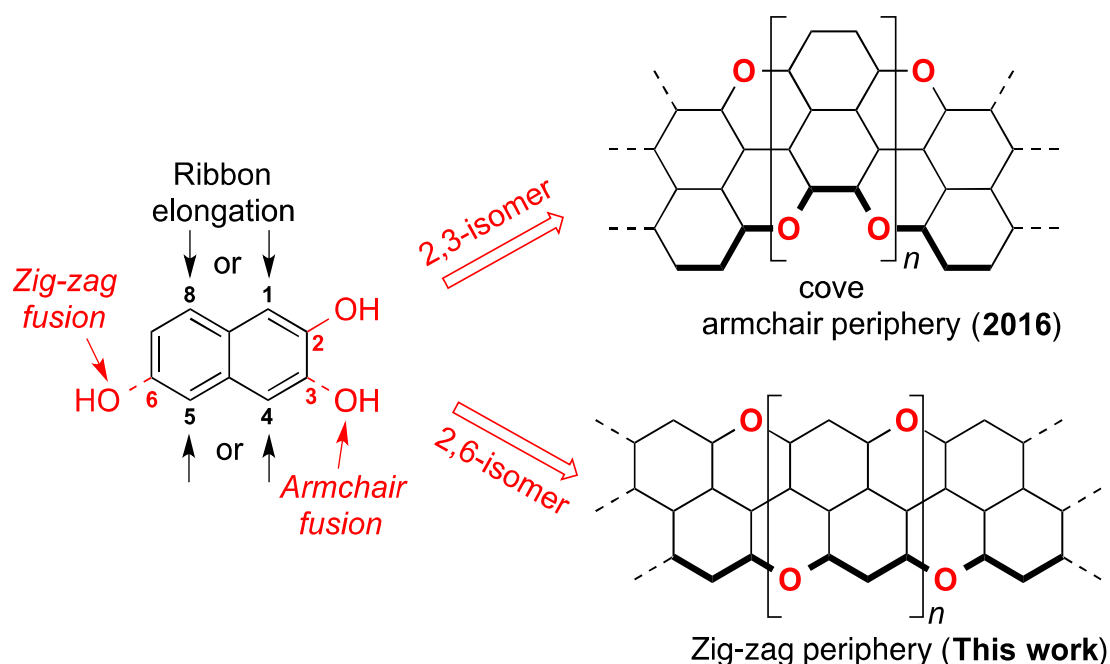
Scheme 1. Engineering O-doped peripheries with armchair and zig-zag topologies.

Recently, we synthesized O-doped benzorylenes featuring cove armchair peripheries from oligonaphthalenes precursors that, made from 2,3-dihydroxynaphthalene and 2-hydroxynaphthalene through Cu-mediated oxidative C-C oligomerization at the C1 and C4 positions, were planarized by oxidative O-annulation (Scheme 1).[18] In studying this synthetic strategy, we noticed that O-doped PAHs featuring zig-zag peripheries could be also prepared (Scheme 1). In fact, we envisioned these PAHs as arising by the oligomerization of 2,6-dihydroxynaphthalene at the C1 and C5 positions followed by the C-O oxidative planarization reaction using an appropriate protection/deprotection management of the

hydroxyl groups. At the synthetic planning level (Scheme 2), these considerations led us to contemplate at first the C1-C5 oligomerization of 2,6-dihydroxynaphthalene and then the oxidative cycloetherification reaction involving the hydroxyl groups at the 2 and 6 positions (path A).
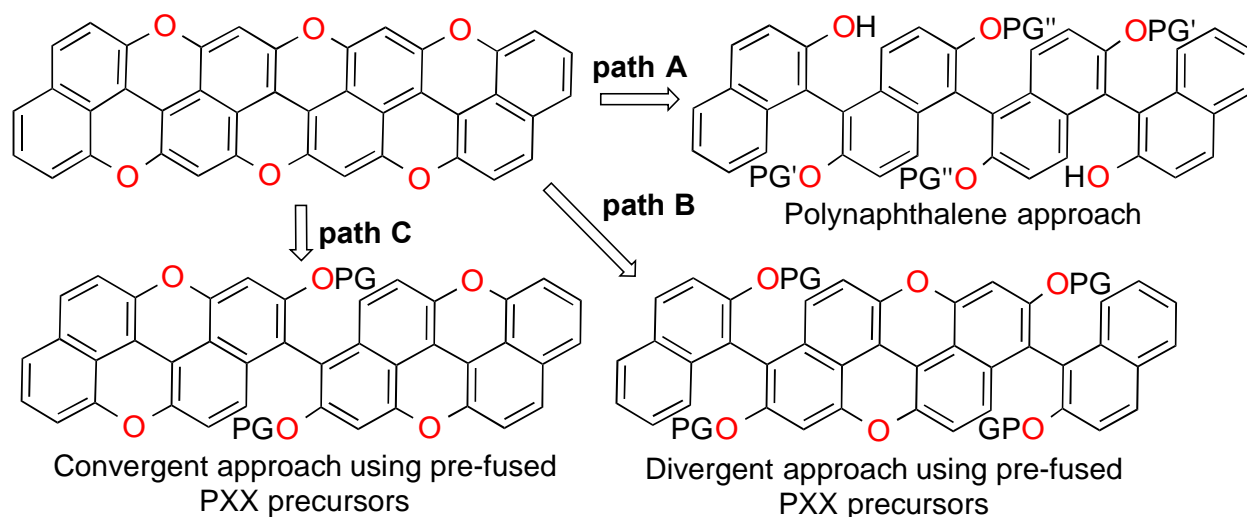
Scheme 2. Synthetic strategies for preparing Zig-zag O-doped peri-acenoacenes. PG: protecting group.

However, the high susceptibility of 2,6-dihydroxynaphthalene and of its protected analogues under oxidative conditions forced us to abandon this path. This led us to consider divergent (path B) and convergent (path C) synthetic strategies using hydroxyl-functionalized PXX precursors, thus relegating an oxidative planarization step at an earlier stage. As we have predicted a potential chemical instability of the dihydroxy-PXX core of divergent path B under oxidation conditions, we decided to undertake convergent plan C. This line of thought led us back to prepare a 2-hydroxy-PXX precursor as the key building unit. Anticipating a strong tendency to form aggregates,[18] xylyl moieties were added.

To commence, dimethoxynaphthalene **2** was reacted with n-BuLi and TMSCl to give TMS-functionalized naphthalene **3** that, upon subsequent treatment with ICl gave desired diiodonaphthalene **4** (Scheme 3).[19] Subsequent Suzuki cross-coupling of **4** with 2,6-

dimethylphenylboronic acid led to **5** (see X-ray structure in Fig. 2a) that, in the presence of n-C$_{12}$H$_{25}$SNa, could be monodeprotected to give naphthol **6** in 65% (see X-ray structure in Fig. S21).
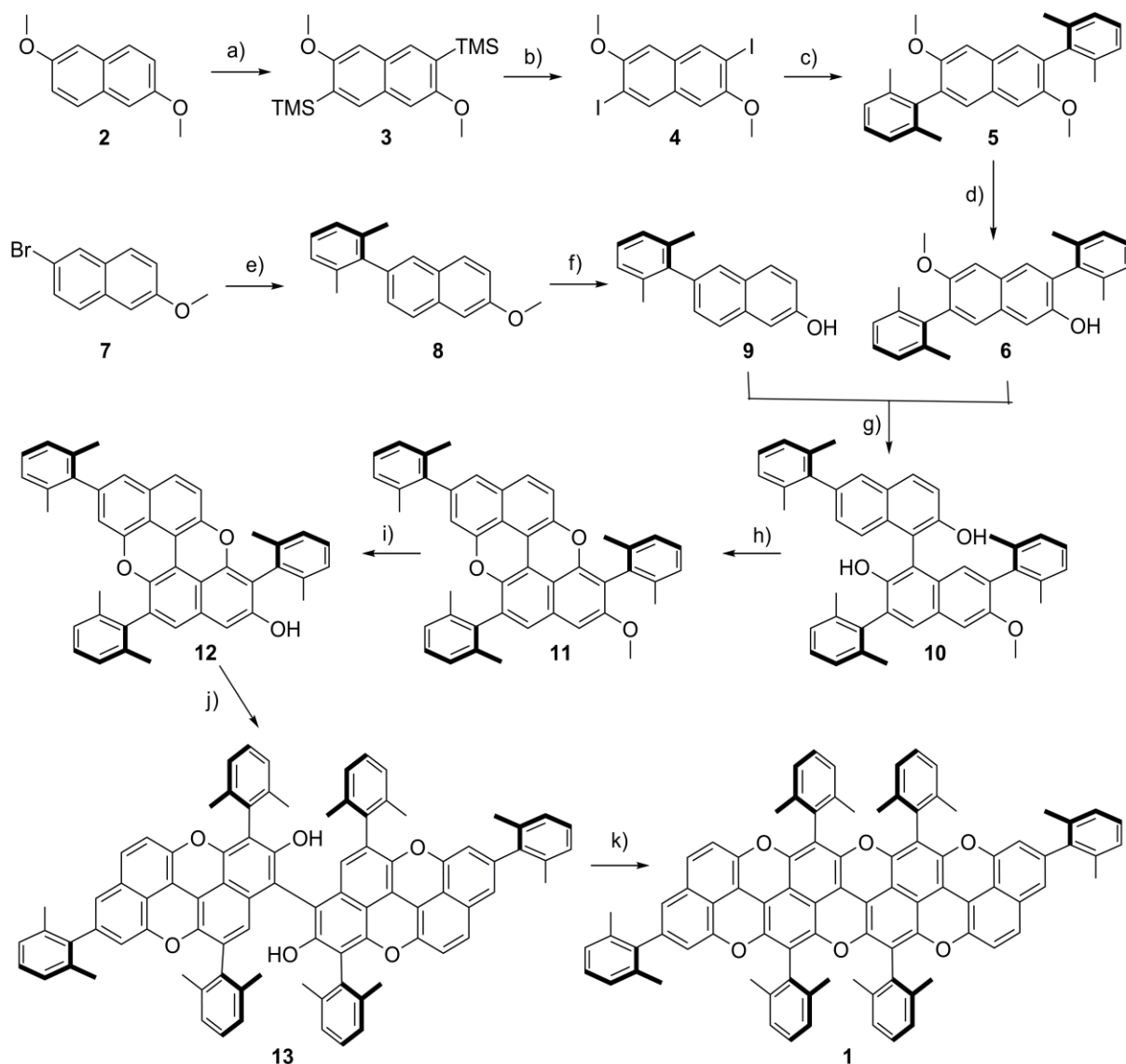
Scheme 3. Synthesis of Zig-zag O-doped peri-acenoacenes **1**. Reagents and conditions: a) [1] n-BuLi/hex (2.4 eq) THF, 0 °C, 3 h; [2] TMSCl (2.4 eq) 0 °C to rt., 2 h; [3] n-BuLi/hex (2.0 eq) 0 °C, 2 h; [4] TMSCl (2.0 eq) 0 °C to rt., 82%; b) ICl (2.1 eq), CH$_2$Cl$_2$, 0 °C to rt., 10 h, 96%; c) 2,6-dimethylphenylboronic acid (6.0 eq), K$_3$PO$_4$ (6.0 eq), SPhos (0.2 eq), Pd(dba)$_2$ (0.1 eq), dioxane/water (5:1), 101 °C, 4 h, 93%; d) n-C$_{12}$H$_{25}$SH (1.1 eq), NaOH (2.2 eq), NMP, 130 °C, 48 h, 77%; e) 2,6-dimethylphenylboronic acid (2.0 eq), K$_3$PO$_4$ (2.0 eq), SPhos (0.2 eq), Pd(dba)$_2$ (0.1 eq), dioxane/water (5:1), 101°C, 12 h, 97%; f) BBr$_3$ (1M in CH$_2$Cl$_2$, 3 eq), CH$_2$Cl$_2$, 0 °C to rt., 12 h, 94%; g) naphthols 1:1, CuCl$_2$ (2 eq), PhCH(NH$_2$)CH$_3$ (2.5 eq), MeOH/ CH$_2$Cl$_2$, 0 °C to rt., 2 h, 35%; h) CuCl (0.3 eq), K$_2$CO$_3$ (2.0 eq), N-methylimidazole (0.6 eq), 120 °C, 20 h, 64%; i) dodecane thiol (3.0 eq), NaOH (5.0 eq), NMP, 130 °C, 4 h, 93%; j) Cu-TMEDA (0.1 eq), CH$_2$Cl$_2$, rt., 5 min, 84%; k) CuCl (0.3 eq), K$_2$CO$_3$ (2.0 eq), N-methylimidazole (0.6 eq), 120 °C, 20 h, 17%.

In parallel, Suzuki cross-coupling reaction between 2-bromo-6-methoxynaphthalene **7** and 2,6-dimethylphenylboronic acid followed

by demethylation with BBr$_3$ gave naphthol **9** with an overall yield of 81%. Subsequent C-C oxidative heterodimerization of **6** and **9** gave binaphthol **10** as a racemic mixture in 35% yield (Scheme 3). Surprisingly, oxidative O-annulation of **10** following our protocol (CuI, PivOH in DMSO at 140 °C)[18] failed, giving **11** with only 7% yield and extensive degradation. However, when using the protocol of Kamei and co-worker, CuCl (cat.) and *N*-methylimidazole (NMI) in *m*-xylene at 120 °C,[20] we could obtain MeO-PXX derivative **11** in 64% yield (see X-ray structure in Fig. 2b). Subsequent removal of the methyl protecting group with *n*-C$_{12}$H$_{25}$SNa gave hydroxy-PXX **12** that, being prone to oxidative degradation, was immediately homodimerized into derivative **13** (78%) in the presence of Cu-TMEDA (10%) in CH$_2$Cl$_2$.[21] Final oxidative ring-closure reaction under Kamei's conditions[20] gave desired zig-zag nanoribbon **1** as an orange solid (Scheme 3). The molecular ion of **1** was identified by HR-MALDI through the detection of the peak at m/z 1214.4518 (C$_{88}$H$_{62}$O$_6$, calc.: 1214.4546, Fig. S19). Solution ^{1}H-NMR spectra further confirmed the structure of **1** (Fig. S18). Whereas the aromatic region is not conclusive due to the overlapping of the proton resonances, a clear indication of the product formation was given in the aliphatic region, with the methyl protons appearing as three singlets (integration 1:1:1) at 2.10, 2.05 and 1.97 ppm. To unequivocally corroborate the chemical structure of **1**, crystals suitable for X-ray diffraction analysis were obtained by hot recrystallization of **1** from toluene (Fig. 2c). The X-ray analysis confirms the flat structure of the zig-zag framework, with C-O lengths varying from 1.383 to 1.416 Å. Given the hindering nature of the xylyl substituents, we could not evidence the presence of any face-to-face π-π stacking interactions and only edge-to-face arrangements, held by C-H···π interactions, were observed (Fig. S20). Similar organizations were also observed for **5** and **11**. All molecules displayed thermal and photochemical stability at the solid state under ambient conditions. To appraise the effect of the O-doping on the aromatic π-surface, we further determined the charge distribution of the crystal structure of **1** in the form of

Electrostatic Surface Potential (ESP, Fig. 3) calculated with Gaussian 09 at B3LYP/6-31G(d,p) level of theory (SI).
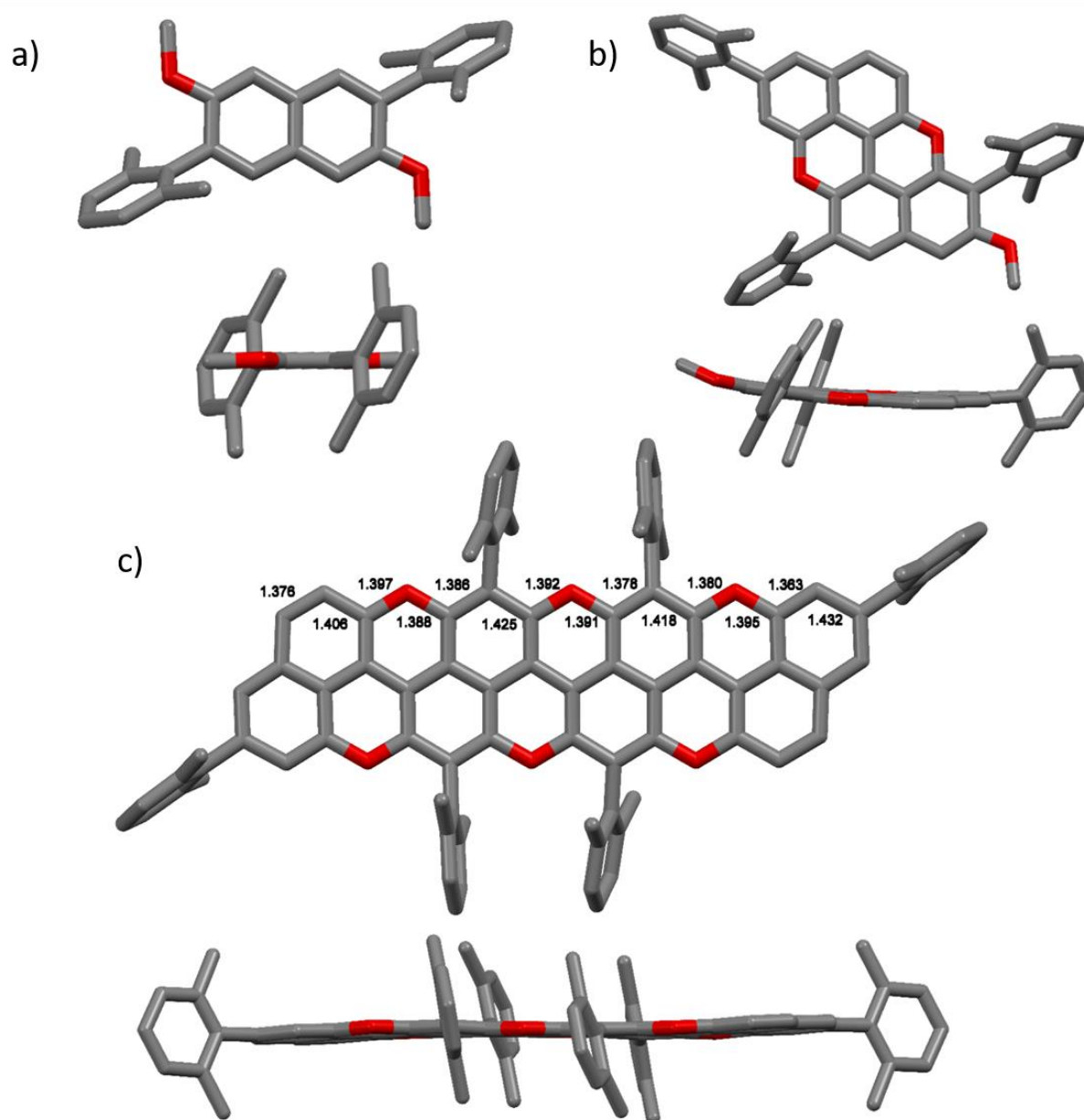
Fig. 2. Top- (top) and side- (bottom) view of the X-ray crystal structures for a) **5** b) **11** and c) **1** (space groups: P-1, P2$_1$/c and P2$_1$/n, respectively). Crystals were obtained from thermal recrystallization from isopropanol (**5**), pentane (**11**) and toluene (**1**).

One can notice that the sequential C-O fusion of the naphthyl monomers leads to a notable charge distribution within the π-surface of the aromatic ribbon, with the negatively charged regions segregated at the two C-edged naphthyl peripheries and O-edges of molecules **11** and **1**. Surprisingly, weakly positively

8

charged areas (Fig. 3, white arrows) appear at the centers of each pyranopyran cycles, suggesting the occurrence of significant charge depletion on the two inner naphthyl rings. These observations likely indicate that the presence of the pyranopyran rings restricts the electron delocalization due to their antiaromatic contribution.
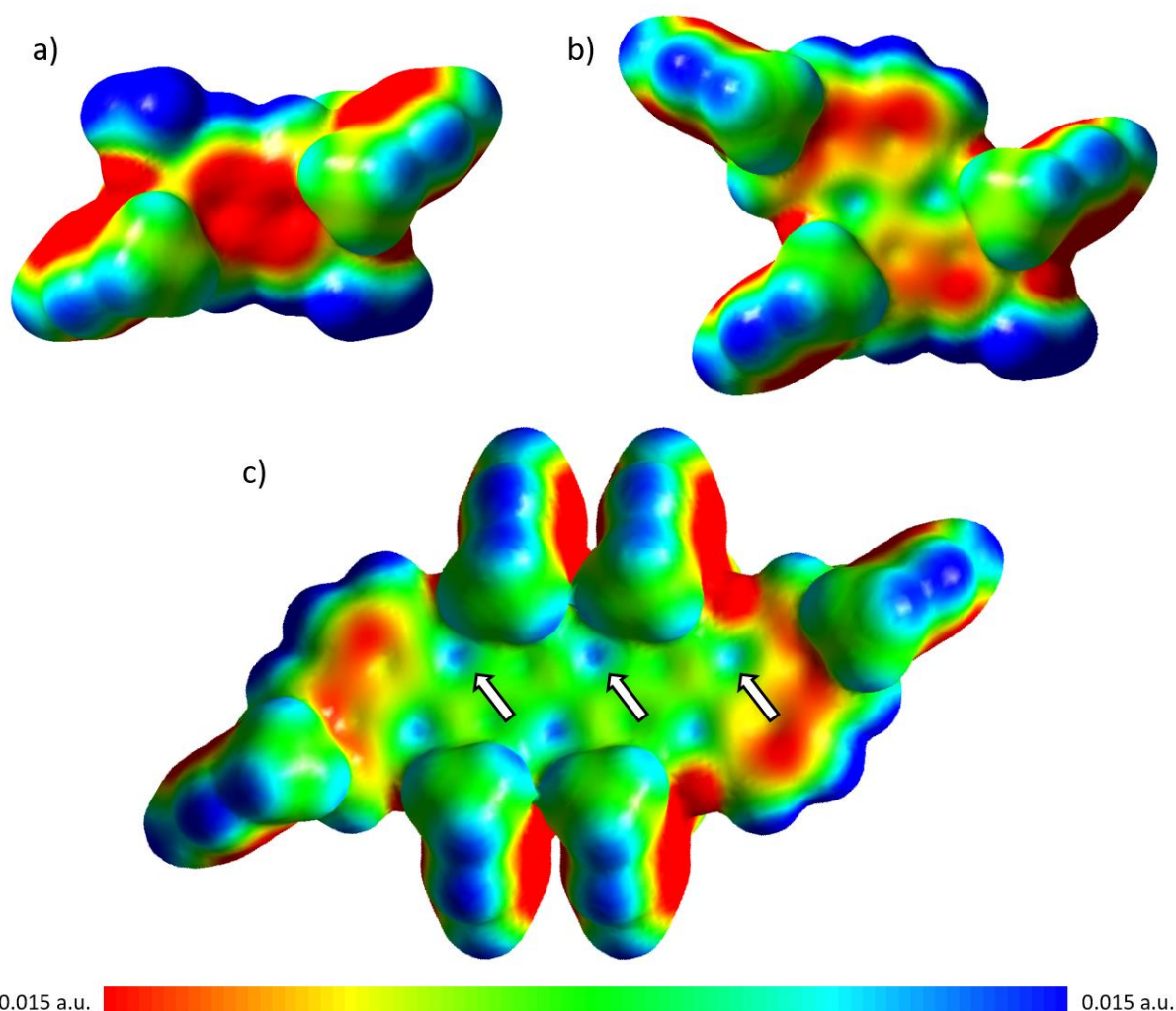
Fig. 3. Electrostatic Surface Potentials (ESP) for a) **5,** b) **11** and c) **1** mapped on the *vdW* surface up to an electron density of 0.001 electron.bohr^{-3}.

UV-vis absorption and emission properties of molecules **1** and **11** and reference **5** in THF are displayed in Fig. 4 and Table 1. The lowest-energy electronic transition of **1** appears in the green region (523 nm) at significantly lower energy than that of **11** (449 nm). This finding suggests that the dimerization and planarization of **11** into **1** causes a contraction of the optical bandgap (ΔE_{opt} = 0.40 eV). Consistently, the emission spectra shown in Fig. 4

reflect the same trend, with the intense emission peak of **1** (λ_{max} = 540 nm, Φ_{fl} = 0.38) significantly red-shifted with respect to that of **11** (λ_{max} = 457 nm, Φ_{fl} = 0.48), with nanosecond lifetimes (Table 1).[10, 22]
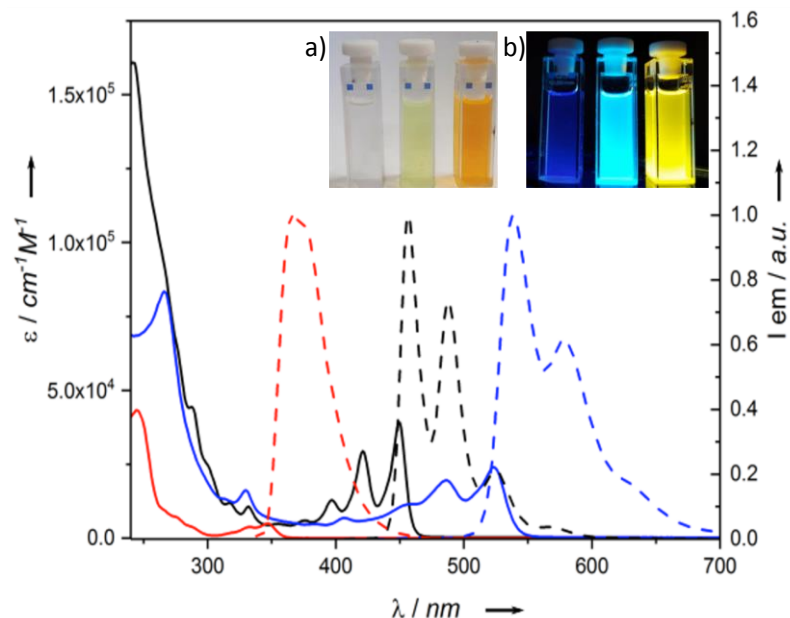
Fig. 4. Absorption (—) and normalized emission (---) spectra of **1** (blue), **5** (black) and **11** (red) in THF at r.t. *Inset:* solutions containing **5**, **11** and **1** in THF a) and b) under UV lamp (λ_{exc} = 254 nm).

Table 1. Photophysical data in THF at r.t. Estimated HOMO-LUMO energy gap (E_g) as determined by optical (E_{00}) and theoretical (E_g^T) studies.

Molecule	Absorption	Emission			Energy Band Gap	
	λ, nm (ε, M^{-1} cm^{-1})	λ_{max} (nm)	τ (ns) [a]	Φ_{fl}[b]	E_{00} (eV) [c]	E_g^T (eV) [d]
5	346 (5000) 332 (3800)	356	6.5	0.48	3.50	4.40
11	449 (39000) 421 (29500) 397 (12900)	457	5.9	0.67	2.74	3.29
1	523 (23900) 486 (19500) 457 (11500)	540	5.1	0.38	2.34	2.78

[a]λ_{ex} = 372 or 459 nm. [b]Standard: C153 in EtOH at r.t. (Φ = 0.53).[23] [b]9,10-Diphenilanthracene in CyH (Φ = 0.97±0.03).[24] [c]Energy (eV) calculated from normalized lowest absorption band and highest emission band cross in nm, exploiting the conversion nm to eV: E_{00} = 1240.5/λ_{cross}. [d]Calculated bandgap value at the B3LYP/6-31G** level of theory, from gas phase optimized geometry.

Next, we examined the redox properties by cyclic voltammetry (CV) measurements and differential pulse (DPV) voltammetry (Table 2 and Fig. S24 and S25). The CV of **5** feature a reversible first oxidation wave at approximately 0.84 V and a second irreversible event around 1.20 V. Both peaks are considerably higher in energy with respect to those observed for **11** (0.35 V). Two reversible monoelectronic redox oxidations with very similar current were instead observed for nanoribbon **1**, at -0.06 and +0.09 V *vs* Fc, respectively. The first and second oxidation peaks each correspond to a 1-e⁻ process, advocating that the first oxidation of **11** splits into two couples for **1** (as it also happens with the irreversible processes). Notably, the first oxidation wave of **1** is negatively shifted by ca. 0.90 and 0.41 V compared to that of **5** and **11**, respectively. No relevant reduction waves were detected at any scan rates for any of the molecules under the same experimental conditions.

Table 2. CV data calculated *vs.* the Fc/Fc⁺ couple in THF at r.t. Peak separations in mV are in brackets. Scan rate: 50 mV/s. Supporting electrolyte: TBAPF₆.

Molecule	$E^{1/2}_{ox,1}$[a]	$E^{1/2}_{ox,2}$[a]	ΔE_{HL}
5	0.84 (90)	1.20[c]	3.50
11	0.35 (93)	0.80[c]	2.74
1	-0.06 (70)	0.09(88)	2.34

[a]Halfwave potentials unless differently specified. [b]Peak potential. [c]Irreversible wave. "nd" stands for "not detected".

Taken together, these physical data allowed us to estimate the energies of the HOMO and LUMO orbitals, resulting to be -4.74 eV (HOMO) and -2.40 eV (LUMO) for **1**, -5.14 eV (HOMO) and -2.41 eV (LUMO) for **11** and -5.64 eV (HOMO) and -2.14 eV (LUMO) for **5** (Fig. 4). The extension of the molecule provokes a rise of the HOMO energy level, making nanoribbon **1** a strong electron donor (i.e., p-type semiconductor). To shed further light on the structure-property relation, we calculated the HOMO and LUMO orbitals for **1**

(Fig. 4). While the LUMO of **1** is mainly located on the central core of the ribbon, both HOMO and LUMO of molecules **5** and **11** are distributed on the entire π-surface.
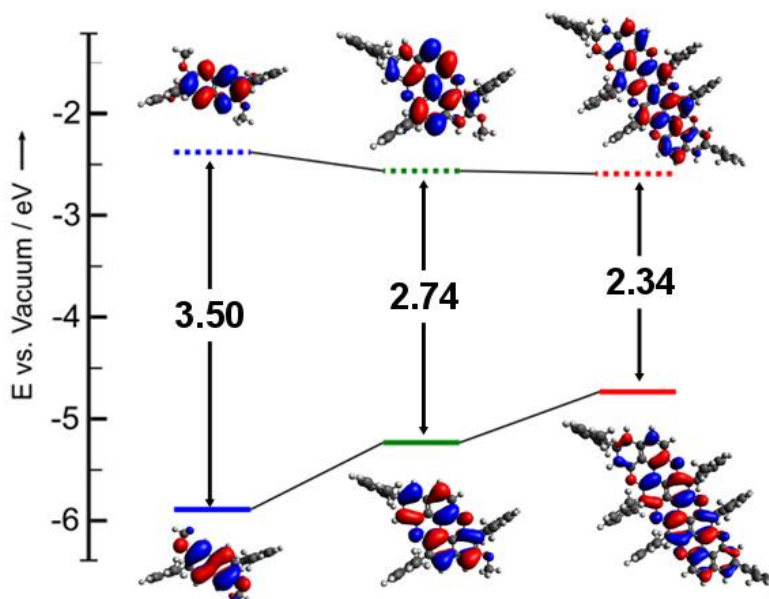

Fig. 5. Frontier orbital energies estimated from the CV and photophysical data for molecules **1**, **5** and **11** together with theirs HOMO and LUMO profiles at B3Lyp/6-31G(d,p) level of theory (gaussian09). Reduction potentials of the excited triplet states are evidenced as the narrower optical energy gaps ($E^{T*} = E^{1/2}_{ox}-E_{opt}^{T}$). Fc^{+}/Fc = 0.46 V vs. SCE; -4.8 eV *vs* vacuum.

In conclusion, in this paper we have described the first synthesis of an unprecedented, chemically and thermally stable, O-doped zig-zag molecular graphenes taking advantage of the formation of pyranopyran rings through an oxidative C-O planarization protocol. UV-vis absorption and emission studies showed that these molecules feature high emission yields and tunable absorption properties throughout the UV-vis spectral region, with the hexaoxo derivative being a green absorber. Electrochemical investigations showed that the progressive extension of the O-annulated framework provokes a shrinking of the HOMO-LUMO energy gap due to a rise in the HOMO energy level. The remarkable chemical stability and electron-donating capabilities make this class of molecules fascinating for the engineering of *p*-type semiconductors. Given the importance to transfer our O-doped molecular graphenes into 1D and 2D materials, we are currently developing novel synthetic approaches that will give access to different doping patterns, extending the current molecular framework into macromolecular ribbons.

References

[1]   a) A. Narita, X.-Y. Wang, X. Feng, K. Müllen, *Chem. Soc. Rev.*
      2015, *44*, 6616; b) X. Wang, G. Sun, P. Routh, D.-H. Kim, W.
      Huang, P. Chen, *Chem. Soc. Rev.* **2014**, *43*, 7067.

[2]   a) U. N. Maiti, W. J. Lee, J. M. Lee, Y. Oh, J. Y. Kim, J. E.
      Kim, J. Shim, T. H. Han, S. O. Kim, *Adv. Mater.* **2014**, *26*, 40;
      b) T. Baumgartner, *Acc. Chem. Res.* **2014**, *47*, 1613; c)
      M. Stępień, E. Gońka, M. Żyła, N. Sprutta, *Chem. Rev.* **2017**,
      117, 3479; d) X.-Y. Wang, J.-Y. Wang, J. Pei, *Chem. Eur. J.*
      2015, *21*, 3528.

[3]   M. Takase, T. Narita, W. Fujita, M. S. Asano, T. Nishinaga,
      H. Benten, K. Yoza, K. Müllen, *J. Am. Chem. Soc.* **2013**, *135*,
      8031.

[4]   L. Junzhi, R. Berger, K. Müllen, X. Feng, in *From
      Polyphenylenes to Nanographenes and Graphene Nanoribbons.
      Advances in Polymer Science, Vol. 278* (Eds.: K. Müllen, X.
      Feng), Springer, Cham, **2017**, pp. 1-32.

[5]   J. R. Dias, *Can. J. Chem.* **1984**, *62*, 2914.

[6]   a) J. E. Anthony, *Angew. Chem., Int. Ed.* **2008**, *47*, 452; b) L.
      Zöphel, R. Berger, P. Gao, V. Enkelmann, M. Baumgarten, M.
      Wagner, K. Müllen, *Chem. Eur. J.* **2013**, *19*, 17821; c) X.
      Zhang, J. Li, H. Qu, C. Chi, J. Wu, *Org. Lett.* **2010**, *12*,
      3946; d) Z. Sun, Q. Ye, C. Chi, J. Wu, *Chem. Soc. Rev.* **2012**,
      41, 7857.

[7]   a) C. Rogers, C. Chen, Z. Pedramrazi, A. A. Omrani, H.-Z.
      Tsai, H. S. Jung, S. Lin, M. F. Crommie, F. R. Fischer,
      Angew. Chem., Int. Ed. **2015**, *54*, 15143; b) P. Ruffieux, S.
      Wang, B. Yang, C. Sánchez-Sánchez, J. Liu, T. Dienel, L.
      Talirz, P. Shinde, C. A. Pignedoli, D. Passerone, T.
      Dumslaff, X. Feng, K. Müllen, R. Fasel, *Nature* **2016**, *531*,
      489; c) J. Krüger, F. García, F. Eisenhut, D. Skidin, J. M.
      Alonso, E. Guitián, D. Pérez, G. Cuniberti, F. Moresco, D.
      Peña, *Angew. Chem., Int. Ed.* **2017**, *56*, 11945.

[8]   a) M. Bendikov, F. Wudl, D. F. Perepichka, *Chem. Rev.* **2004**,
      104, 4891; b) J. E. Anthony, *Chem. Rev.* **2006**, *106*, 5028; c)
      R. A. Pascal, *Chem. Rev.* **2006**, *106*, 4809.

[9]   a) S. Ullah, P. A. Denis, F. Sato, *ChemPhysChem* **2017**, *18*,
      1864; b) R. Szűcs, P.-A. Bouit, L. Nyulászi, M. Hissler,
      ChemPhysChem **2017**, *18*, 2618.

[10] a) C. Song, T. M. Swager, *Macromolecules*, **2009**, *42*, 1472; b)
      T. Miletic, A. Fermi, I. Orfanos, A. Avramopoulos, F. De
      Leo, N. Demitri, G. Bergamini, P. Ceroni, M. G. Papadopoulos,
      S. Couris, D. Bonifazi, *Chem. Eur. J.* **2017**, *23*, 2363; c) A.
      Sciutto, A. Fermi, A. Folli, T. Battisti, J. M. Beames, D. M.
      Murphy, D. Bonifazi, *Chem. Eur. J.*, DOI
      10.1002/chem.201705620.

[11] a) C. Bronner, S. Stremlau, M. Gille, F. Brauße, A. Haase, S.
      Hecht, P. Tegeder, *Angew. Chem., Int. Ed.* **2013**, *52*, 4422; b)
      R. Berger, A. Giannakopoulos, P. Ravat, M. Wagner, D.
      Beljonne, X. Feng, K. Müllen, *Angew. Chem., Int. Ed.* **2014**,
      53, 10520; c) Y. S. Park, D. J. Dibble, J. Kim, R. C. Lopez,
      E. Vargas, A. A. Gorodetsky, *Angew. Chem., Int. Ed.* **2016**, *55*,

3352; d) D. Cortizo-Lacalle, J. P. Mora-Fuentes, K. Strutyński, A. Saeki, M. Melle-Franco, A. Mateo-Alonso, *Angew. Chem., Int. Ed.* **2018**, *57*, 703.

[12] a) T. Katayama, S. Nakatsuka, H. Hirai, N. Yasuda, J. Kumar, T. Kawai, T. Hatakeyama, *J. Am. Chem. Soc.* **2016**, *138*, 5210; b) X.-Y. Wang, A. Narita, W. Zhang, X. Feng, K. Müllen, *J. Am. Chem. Soc.* **2016**, *138*, 9021; c) M. Numano, N. Nagami, S. Nakatsuka, T. Katayama, K. Nakajima, S. Tatsumi, N. Yasuda, T. Hatakeyama, *Chem. Eur. J.* **2016**, *22*, 11574.

[13] X. Wang, F. Zhang, K. S. Schellhammer, P. Machata, F. Ortmann, G. Cuniberti, Y. Fu, J. Hunger, R. Tang, A. A. Popov, R. Berger, K. Müllen, X. Feng, *J. Am. Chem. Soc.* **2016**, *138*, 11606.

[14] M. Fingerle, C. Maichle-Mössmer, S. Schundelmeier, B. Speiser, H. F. Bettinger, *Org. Lett.* **2017**, *19*, 4428.

[15] R. Pummerer, E. Prell, A. Rieche, *Berichte der deutschen chemischen Gesellschaft (A and B Series)* **1926**, *59*, 2159.

[16] N. Lv, M. Xie, W. Gu, H. Ruan, S. Qiu, C. Zhou, Z. Cui, *Org. Lett.* **2013**, *15*, 2382.

[17] N. Kobayashi, M. Sasaki, K. Nomoto, *Chem. Mater.* **2009**, *21*, 552.

[18] D. Stassen, N. Demitri, D. Bonifazi, *Angew. Chem., Int. Ed.* **2016**, *55*, 5947.

[19] M. Chikahiko, S. Junshi, M. Kazumoto, S. Kazutaka, O. Yoshinori, T. Hayato, T. Jun, N. Eiichi, *Bull. Chem. Soc. Jpn.* **2015**, *88*, 776.

[20] T. Kamei, M. Uryu, T. Shimada, *Org. Lett.* **2017**, *19*, 2714.

[21] S. Bhushan, K. Vijayakumaran, *Acros Organics Review* **2001**, 7.

[22] R. Al-Aqar, A. C. Benniston, A. Harriman, T. Perks, *ChemPhotoChem* **2017**, *1*, 198.

[23] C. Würth, M. Grabolle, J. Pauli, M. Spieles, U. Resch-Genger, *Nat. Protoc.* **2013**, *8*, 1535.

[24] K. Suzuki, A. Kobayashi, S. Kaneko, K. Takehira, T. Yoshihara, H. Ishida, Y. Shiina, S. Oishi, S. Tobita, *Phys. Chem. Chem. Phys.* **2009**, *11*, 9850.